Phys Chem Minerals (2003) 30: 382–392
DOI 10.1007/s00269-003-0324-4

ORIGINAL PAPER

C. I. Sainz-Diaz · E. J. Palin
A. Hernández-Laguna · M. T. Dove

Octahedral cation ordering of illite and smectite. Theoretical exchange potential determination and Monte Carlo simulations

Received: 2 August 2002 / Accepted: 23 April 2003

Abstract The distributions of Al^{3+}/Mg^{2+} and Al^{3+}/Fe^{3+} were studied in the octahedral sheet of illites and smectites. Cation exchange interaction parameters J_i, as first, second, third and fourth neighbours were calculated by means of empirical interatomic potentials. Several compositions with different interlayer cations and tetrahedral charge were studied in both Al/Mg and Al/Fe systems. The values of J_i parameters were similar in all Al/Mg samples. From these J_i values, a strong trend to form AlMg pairs was observed in the Al/Mg system. In the Al/Fe system, the values of J_i are very small, indicating no preference for Al/Fe mixing. From these J_i parameters, Monte Carlo simulations of octahedral cation ordering were performed. In the Al/Mg system, an order/disorder phase transition was observed obtaining a fully ordered distribution without presence of an MgMg pair, according to experimental data. Similar phase transitions were observed for the octahedral compositions Al/Mg 1/1 and 3/1. In the Al/Fe system an order/disorder phase transition was also detected but at very low temperature for illite and smectite. Complete Al/Fe mixing is observed in the most stable ordered distribution. This is consistent with experimental results for synthetic Fe/Al smectites.

Keywords Cation ordering · Illite · Smectite · Monte Carlo simulations

C. I. Sainz-Diaz (✉) · A. Hernández-Laguna
Estación Experimental del Zaidín (CSIC),
C/ Profesor Albareda, 1. 18008-Granada (Spain)
Fax: +34–958129600
e-mail: sainz@lec.ugr.es

E. J. Palin · M. T. Dove
Department of Earth Sciences,
University of Cambridge, Downing Street,
Cambridge CB2 3EQ, UK

Introduction

A great diversity of 2:1 phyllosilicates exists in nature because they can present a wide range of cation composition in the octahedral and tetrahedral sheets. In dioctahedral 2:1 phyllosilicates, isomorphous substitution of Al^{3+} by Mg^{2+} in the octahedral sheet or Si^{4+} by Al^{3+} in the tetrahedral sheet results in a net negative charge that is balanced by the presence of cations in the interlayer space. Determination of the distribution of cations within the sheets is a complex problem, especially in the octahedral sheet, to which we refer in this paper. This type of study can be useful to understand natural processes, such as smectite to illite transformation, and to analyze how cation distribution affects lattice stability. Also, the industrial applications of smectite due to its valuable catalytic and adsorptive properties (e.g. as a barrier in nuclear waste and pollutant disposal repositories) make it of great interest to establish a firm theoretical understanding of their structure and behaviour.

The phenomenon of cation ordering in aluminosilicate minerals has been one of the important aspects of mineral behaviour for a long time, particularly since it can have a significant effect on the thermodynamic properties. The cation distribution for the octahedral sheet of phyllosilicates has been studied experimentally. Besson et al. (1987) found from IR studies that octahedral cation distribution is not random and Al^{3+} and Fe^{3+} tend to segregate from each other. Using ^{27}Al NMR on montmorillonite, Morris et al. (1990) found that Fe was either segregated from Al in the octahedral sheet or present in a phase different from smectite. Grauby et al. (1991, 1993) synthesized smectites with different proportions of Al^{3+}, Mg^{2+} and Fe^{3+}. They studied how these cations arrange in the octahedral sheet using IR and found that Al^{3+} and Fe^{3+} tend to mix rather than to segregate, Mg^{2+} and Fe^{3+} to segregate within the same layer and Mg^{2+} and Al^{3+} to segregate, creating dioctahedral and trioctahedral layers. Schroeder

(1993) studied shale illite-smectite (I–S) samples using ^{27}Al NMR, and found that Fe mixes with Al in samples with low Fe content but Fe segregates from Al in Fe-rich specimens. Drits et al. (1997) studied the isomorphous cation distribution in celadonites, glauconites and Fe-illites by IR, Mössbauer and EXAFS spectroscopies together with simulations by probabilistic methods, finding a certain short-range ordering. Muller et al. (1997) studied octahedral cation distribution of the Camp-Bertaux montmorillonite using XRD, EXAFS and FT-IR, and observed that Mg and Fe form clusters that segregate from Al. Therefore, some discrepancies are found and no definitive conclusion can be extracted from this experimental work.

Computer simulations can play a useful role in these studies. Atomistic calculations with interatomic empirical potentials to represent the short-range interaction between atoms have reproduced the structure and properties of aluminosilicates, particularly phyllosilicates (Collins and Catlow 1992; Sainz-Díaz et al. 2001a). These calculations are useful for the determination of ordering energies (Dove et al. 1993, 1996; Thayaparam et al. 1996; Bosenick et al. 2000, 2001, Palin et al. 2001). Monte Carlo (MC) simulations have been shown to be a powerful tool for the study of cation distribution and ordering in minerals. These methods have been used in aluminosilicates (Herrero and Ramírez 1992; Herrero 1993; Dove and Heine 1996; Dove et al. 1996; Warren et al. 2001). Previous studies (Cuadros et al. 1999; Sainz-Díaz et al. 2001b) of octahedral cation (Al, Fe and Mg) distribution in a series of illite–smectite (I–S) mixed-layer samples using FT–IR data and inverse Monte Carlo calculations, contrasted with ^{27}Al MAS NMR data, showed Fe segregation by short-range Fe ordering. The confusion found in the experimental behaviour explanations of the order–disorder of octahedral cations in clays urges us to study this phenomenon theoretically. Calculations for most illitic specimens, however, suggested medium- or long-range Fe ordering. In this work, the ordering of Al/Mg and Al/Fe octahedral systems is studied from atomistic modelling calculations, determining theoretical cation exchange potential and performing MC simulations.

Methods

For the cation-ordering simulations we compute firstly the ordering interactions by means of interatomic potentials and lattice energy relaxation methods and then we use Monte Carlo methods to simulate the ordering process.

Interatomic potential model

The basic interatomic potential model was described previously elsewhere (Collins and Catlow 1992; Bosenick et al. 2001; Palin et al. 2001; Sainz-Díaz et al. 2001a). These potentials are Coulomb interactions between the ionic charges and a short-range function, which describes the non-Coulombic interactions between ions, that is the Pauli repulsion at short range and the dispersion forces at longer ranges (Abbot et al. 1989a,b).

Electrostatic Coulomb interactions are evaluated by the Ewald method using formal charges on all atoms, except for the OH species, whose component atoms have partial charges chosen so as to reproduce the dipole moment of the OH group. The short-range cation/oxygen interactions are described by Buckingham potentials:

$$E = A\exp(-r/\rho) - Cr^{-6} \quad , \tag{1}$$

where the exponential and the r^{-6} terms describe the repulsive energy and the longer-range attraction, respectively. The parameters A, ρ and C are described in Table 1.

In the modelling of all oxygen atoms, except those from hydroxyl groups, electronic polarizability effects are taken into account by using the shell model. In this model the atoms are considered to consist of a core comprising the nucleus and tightly bound inner electrons, surrounded by a massless shell of the remaining outer electrons. The core is assigned a charge of $+ 0.84819e$ and the shell a charge of $- 2.84819e$, maintaining the formal value for the overall ionic charge. The shell and core are held together by an ideal harmonic core–shell interaction:

$$E = 1/2K_s r^2 \quad , \tag{2}$$

where K_s is the harmonic spring constant and r is the separation between the centres of core and shell.

The O and H atoms within the hydroxyl group are given non-formal charge values, although the overall charge on the hydroxyl molecular ion has a formal charge of − 1e. The intramolecular OH interaction is described by a Morse potential:

$$E = D\{1 - \exp[-a(r-\mu)]\}^2 \quad , \tag{3}$$

where r and μ are the observed and equilibrium interatomic distances, respectively. The parameters D and a are described in Table 1. Coulomb forces are not included between atoms coupled by a Morse potential, as it is assumed that this potential describes all components of the interactions between both atoms.

Covalent effects are simulated using three-body bond-bending interactions:

$$E = 1/2k(\theta - \theta_0)^2 \quad , \tag{4}$$

where k is the harmonic three-body force constant, and θ and θ_0 are the observed and ideal bond angles, respectively.

The values of the parameters for the potentials used in this work are described in Table 1. An empirical Al^{3+}–O^{2-} potential has been used for all coordinations (Jackson and Catlow 1988). Although the OH groups are joined to cations of the octahedral sheet, they are also close to the cations of the tetrahedral sheet. Then, we include an empirical Si^{4+}_{core}–$O^{1.426-}_{core}$ potential for the Si/OH interactions (Collins and Catlow 1992). Since the isomorphous substitutions of Mg and Fe occur in the octahedral sheet, the Mg–O and Fe–O potentials were also included for both types of oxygens (O^{2-} and OH). The longer-range H bonds (OH…O) are described by an H–O Buckingham potential (Winkler et al. 1991). For modelling the interlayer space interactions with exchange cations, the K–O potential from Post and Burnham (1986), the Na–O potential from Bush et al. (1994) (Bosenick et al. 2000) described quite well the interlayer interactions. All these parameters have been used to model accurately structures and crystal properties of the main rock-forming silicate minerals and layer 2:1 phyllosilicates, and particularly smectites and illites (Sainz-Díaz et al. 2001a). All lattice energy calculations have been performed by means of the GULP code with the Newton–Raphson minimization method for the lattice relaxation (Gale 1997).

Previous theoretical and experimental studies on micas with low tetrahedral Al content found a non-ordered distribution of the cations in the tetrahedral sheet with the Loewenstein rule of AlAl pair avoidance (Herrero and Sanz 1991; Warren et al. 2001). Then, this random distribution was also included in this work by imposing partial occupancies of Si and Al in the crystallographic positions of the tetrahedral sheet.

Table 1 Parameters of the potential set model used in this work

Short-range interactions[a]	A (eV)	ρ (Å)	C (eV Å^{-6})	Reference
Si^{4+}–O^{2-}	1283.9073	0.3205	10.6616	[b]
Si^{4+}–$O^{1.426-}$	999.98	0.3012	0.0	[b]
Al^{3+}–$O^{1.426-}$	1142.6775	0.2991	0.0	[c]
Al^{3+}–O^{2-}	1460.3	0.2991	0.0	[b]
Fe^{3+}–O^{2-}[d]	3219.335	0.2641	0.0	[e]
Mg^{2+}–$O^{1.426-}$	1142.6775	0.2945	0.0	[b]
Mg^{2+}–O^{2-}	1428.5	0.2945	0.0	[b]
K^{+}–O^{2-}	65269.71	0.2130	0.0	[b]
Na^{+}–O^{2-}	1271.504	0.3000	0.0	[e]
O^{2-}–O^{2-}	22764.0	0.149	27.88	[b]
$H^{0.426+}$–O^{2-}	325.0	0.25	0.0	[b]
Short-range interactions[f]	D (eV)	a (Å^{-1})	μ (Å)	
$H^{0.426+}$–$O^{1.426-}$	7.0525	2.1986	0.9485	[b]
Shell–core interaction	K (eV Å^{-2})			
$O^{0.86902-}_{core}$–$O^{2.86902-}_{shell}$	74.92			[b]
Three-body bond-bending[g]	k (eVrad^{-2})	θ_0 (^{0})		
O^{2-}–Si^{4+}–O^{2-}	2.09724	109.47		[b]
O^{2-}–Al^{3+}(T) – O^{2-}	2.09724	109.47		[b]
O^{2-}–M(Oc) – O^{2-}	2.09724	90		[b]
O^{2-}–M(Oc) – $O^{1.426-}$	2.09724	90		
$O^{1.426-}$–M(Oc) – $O^{1.426-}$	2.09724	90		

[a] Parameters for the Buckingham potentials between cation cores and oxygen shells. When the parameter $C = 0.0$, the function takes the form of Born-Mayer potentials. Cutoff at 12 Å
[b] Winkler et al. (1991)
[c] Schröder et al. (1992)
[d] With O^{2-}_{shell}–$O^{1.426-}_{core}$
[e] From Bush et al. 1994
[f] Modified Morse potential between cores
[g] *T* in the tetrahedral sheet; *Oc* in the octahedral coordination: *M* any cation in the octahedral sheet, Al^{3+}, Fe^{3+} and Mg^{2+}

Simulation cell

Smectites of different compositions were studied (Table 2). A unit cell of smectite had been previously optimized by GULP (Gale 1997) allowing relaxation of volume from an experimental geometry (Tsipursky and Drits, 1984). From this optimized unit cell, a supercell of $2 \times 2 \times 1$ was built with periodic boundary conditions. This supercell includes 164 atoms and 16 octahedral sites. All configurations of this supercell with different compositions and cation distributions were optimized, allowing the relaxation of the atomic positions and the cell parameters simultaneously.

Series of 90 random configurations were generated using a computer program (MCCLAY99) described previously by Cuadros et al. (1999). Additionally, six ordered configurations were included in the simulation series (Fig. 1).

Determination of exchange interactions

The energy related to the ordering interactions can be extracted from the above lattice energy calculations of these configurations. In these configurations different relative positions can be defined for the different octahedral sites as first-, second-, third- and fourth-nearest neighbours, according to the shortest different interatomic distances in the crystal (Fig. 2). Considering the radial distribution function in this two-dimensional model, the intercationic distances can be classified in different ranges: < 3.3, 5.1–5.3, 5.8–6.2 and 7.7–8.2 Å, defining the first, second, third and fourth neighbours, respectively. The approach makes use of a model Hamiltonian for the ordering interactions. Taking into account separate pair interactions for two ordering cations, the energy of each configuration can be expressed as

$$H = E_0 + \sum_n \left(N^n_{\mathrm{Al-Al}} E^n_{\mathrm{Al-Al}} + N^n_{\mathrm{M-M}} E^n_{\mathrm{M-M}} + N^n_{\mathrm{Al-M}} E^n_{\mathrm{Al-M}} \right) , \quad (5)$$

where n indicates different types of neighbouring pairs of cations, N is the number of cation pairs for each type, E is the partial energy related with this cation pairing, M is Mg^{2+} or Fe^{3+}, and the total energy requires summation over all types of interactions. E_0 is a constant that indicates all other components of bond energies and any energy that has no effect on the ordering process. The separate energy terms for each neighbour pair can be combined into a single parameter called the exchange parameter (J). This parameter indicates the energy associated with the exchange of two cations to form AlAl and M–M linkages instead of two Al–M linkages. Then this energy expression can be reduced to:

Table 2 Chemical composition and lattice parameters calculated of the samples studied. Structural formulae on the unit-cell basis for $O_{20}(OH)_4$[a]

Sample	Si^{4+}	Al^{3+} (T)[b]	Al^{3+} (Oc)[b]	Mg^{2+}	Fe^{3+}	IC[b]	a	b	c	β
1	7.72	0.28	3	1		$K_{1.28}$	5.22(1)	8.91(2)	10.14(5)	102.5(3)
2	7.72	0.28	3	1		$Na_{1.28}$	5.22(1)	8.91(1)	10.18(2)	105.1(3)
3	7.2	0.8	3	1		$K_{1.8}$	5.22(1)	8.93(1)	10.03(2)	102.4(2)
4[c]	7.72	0.28	3		1	$K_{0.28}$	5.24(1)	8.90(2)	9.54(3)	96.0(2)
5	7.2	0.8	3		1	$K_{0.8}$	5.22(0)	8.93(1)	10.24(1)	102.5(1)

[a] *Values in brackets* represent the standard error in the last figure. Experimental values for similar composition are: $a = 5.18$ Å, $b = 8.98$ Å, $c = 10.08$–10.13 Å, $\beta = 100.2$–$101.4°$ (Tsipursky and Drits, 1984)
[b] *T* Tetrahedral; *Oc* octahedral; *IC* interlayer cation
[c] The values from calculation of unit cell with the virtual crystal approximation are: $a = 5.22$ Å, $b = 8.73$ Å, $c = 10.1$ Å, $\beta = 100.9°$

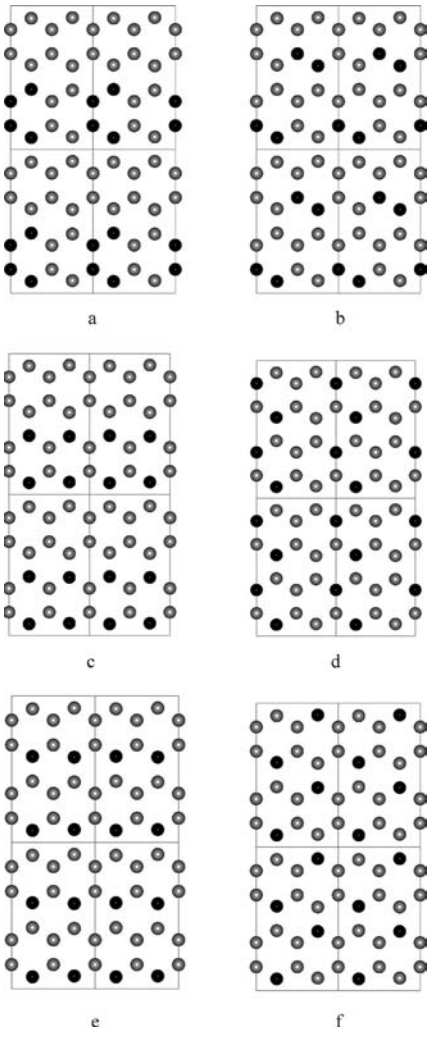

Fig. 1a–f Ordered cation distributions included in the configuration set for calculating the exchange interaction parameters

$$H = E_0 + \sum_n N^n_{\mathrm{Al-Al}}(E^n_{\mathrm{Al-Al}} + E^n_{\mathrm{M-M}} - 2E^n_{\mathrm{Al-M}}) \ . \tag{6}$$

This equation can be used for the determination of the exchange interactions J with the equation:

$$H = E_0 + \sum_n N^n_{\mathrm{Al-Al}} J_n \ . \tag{7}$$

To proceed with the statistical analysis of the energies, it is useful to define an ordering variable (σ) for each site. We take the value $\sigma = -1$ if the site is occupied by Al and $\sigma = +1$ if the site is occupied by M ($\mathrm{M} = \mathrm{Mg}^{2+}$ or Fe^{3+}). Then we can express the energy in terms of the following Hamiltonian model:

$$H = E_0 + \sum_n \sum_{<ij>} \sigma_i \sigma_j J_n \ , \tag{8}$$

where $\langle ij \rangle$ shows that the sum is over all relevant pairs of octahedral sites avoiding the count of any pair twice. The Hamiltonian model holds for all values of the Al:Mg and Al:Fe ratios of the octahedral sheet. A more detailed discussion has been given elsewhere (Bosenick et al. 2001). This model is particularly amenable for analysis by statistical mechanics tools such as the Monte Carlo method used in this work.

For each configuration, all KL cation pairs ($\mathrm{K} = \mathrm{Al}^{3+}$, Mg^{2+} and Fe^{3+}, and $\mathrm{L} = \mathrm{Al}^{3+}$, Mg^{2+} and Fe^{3+}) as first- , second- , third- and fourth-nearest neighbours were calculated by means of the same computer program given above (MCCLAY99; Cuadros et al. 1999). The energy minimization of the different configurations generated provides 90 different lattice energies, which formed a set of values for E in Eq. (6). These energies and the number of Al–Al interactions of each exchange pair for each configuration calculated by our program generated 90 equations of the form of Eq. (6) with the values of E_0 and exchange interactions to be determined by multiple regression analysis.

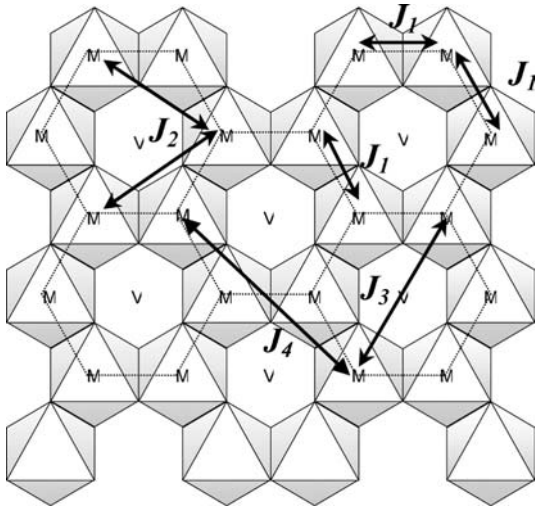

Fig. 2 Definition of the exchange interactions between cation neighbours within an octahedral layer

Monte Carlo simulation

We use the Monte Carlo (MC) method for statistical analysis of the Hamiltonian of Eq. (8). For this work, we used the Ossia code (Warren et al. 2001). This code was written for use on large parallel computers, with the intention of performing parallel simulations of many different temperatures. Further details of Ossia can be found on the WWW at www.esc.cam.ac.uk/ossia.

The MC simulation program does not give information about the structure of the crystal, but about the topology of the bonds between sites. The configuration is defined in terms of a lattice of unit cells, as in a crystal. Each unit cell contains a set of labelled cation sites. Periodical boundary conditions were applied to the simulation cell. Each configuration is defined by the set of cation pairs as first- , second- , third- and fourth-nearest neighbours and by the energy (H) of the Hamiltonian of Eq. (8). The starting configuration for the MC simulation can be random or an ordered distribution. In this configuration, two cations are selected randomly and their positions are exchanged if this action lowers the H value. If H increases the cation positions are exchanged with a probability $\exp(-H/T)$, where T is a relative value of temperature. Each MC step is completed when all cations of the simulation cell have been exchanged. This step is repeated many times (10^6–10^8 times). In a first period, H decreases until the system reaches the equilibrium. Then, H oscillates slightly around the minimum value and all data and average values are taken in this period. This procedure was repeated at different T (20 different T values), following a warming or a cooling process in order to avoid false minimum states.

The output of the MC runs includes a number of expectation values, including $\langle E \rangle$ and $\langle E^2 \rangle$ for the energy. From these values it is possible to form the heat capacity C:

$$C = \frac{\langle E^2 \rangle - \langle E \rangle^2}{K_B T^2} \ . \tag{9}$$

The configurations produced by the MC simulation were monitored by using the Cerius^2 crystal visualizer program. This enabled the identification of ordered configurations, and in par-

ticular identified cases where ordering was accompanied by the formation of domain microstructures.

Results

Ordering energy

Different smectite models were considered in this work. For the Al/Mg ordering study, an octahedral composition Al/Mg = 3/1 was included. Different compositions with tetrahedral charges 0.28 and 0.8 per unit cell, and two interlayer cations (K^+ and Na^+) were selected. For the Al/Fe ordering study an octahedral composition of Al/Fe = 3/1 was also considered, and two different tetrahedral charges were included (0.28 and 0.8 per unit cell) (Table 2).

The unit cell of these samples was previously optimized by using the virtual crystal approximation (VCA, by imposing partial occupancies in all cation sites). These calculated structures have lattice parameters similar to the experimental values, as in previous studies (Sainz-Díaz et al. 2001a). In the $2 \times 2 \times 1$ supercells, the octahedral sites have real occupancies of cations. The supercells were fully optimized, including lattice parameter optimization (relaxation of volume). These optimized supercells yielded lattice parameters similar to the structures calculated with the VCA method, although in sample 4 the calculated parameters c and β are smaller than the experimental ones (Table 2). In this sample the interlayer charge is too low and hence the interactions existing in this interlayer space are too weak to be described perfectly with the empirical potential model used in this work. Nevertheless, the differences are not significant, and the composition of this model is so different to that of natural samples that this compositional variation could justify the difference in the parameters.

Taking into account all configurations calculated for each model, no significant effect of the cation distribution on the lattice parameters was observed, obtaining low standard deviations for each parameter value (Table 2). In the Al/Mg systems the increase in tetrahedral charge (samples 1 and 3) produces a decrease in calculated parameter c, in accord with previous studies (Sainz-Díaz et al. 2001a). The increase in interactions in the interlayer space, produced by the increase of tetrahedral charge, causes a decrease in the interlayer space.

The energy of the ordered configurations (Fig. 1) for different samples is presented in Table 3. In the Al/Mg system the configurations with presence of MgMg pairs (a and b in Table 3) have high energy and they are clearly disfavoured. On the contrary, the configuration with Mg dispersed along the sheet (f) has the lowest energy and it is favoured. These energy differences between these ordered distributions are similar with K^+ or Na^+ as interlayer cations (samples 1 and 2). In the Al/Fe system, the energy sequence is similar, the configuration f is more stable than a, but the energy differences are very small, in the range of 0.01 eV, nearly 20 times lower than in the Al/Mg system.

The optimized geometry of all configurations used for the J set calculation was checked in order to avoid unrealistic internal deformations. All configurations calculated in each sample were fitted to the Hamiltonian model of Eq. (7), obtaining different exchange interactions (J_i, Table 4). Initially, we considered a maximum distance of these interactions of 6.6 Å (only J_1, J_2 and J_3), but the MC simulations with these Js suggested including also the interaction between fourth-order nearest-neighbour cations J_4 (Fig. 2). Good-quality fittings were obtained yielding low standard errors in the values for E_o and Js (Table 4). In some cases, the errors are relatively large due to correlation effects, but these errors do not imply that the values are statistically insignificant. The quality of the agreement between the lattice energy values of the different configurations and the predicted values by means of the Hamiltonian model is shown in Fig. 3.

The samples 1–3 present values of J_i similar to each other. The exchange of Na^+ by K^+ as interlayer cation

Table 3 Energy (eV) of some ordered configurations for the samples studied (Fig. 1)

Sample\distribution	*a*	*b*	*c*	*d*	*e*	*f*
1	−5284.53	−5285.42	−5286.13	−5286.27	−5286.27	−5286.42
2	−5284.02	−5284.86	−5285.60	−5285.71	−5285.71	−5285.86
3	−5207.91	−5208.23	−5208.95	−5209.15	−5209.13	−5209.35
4	−5375.46	−5375.51	−5375.51	−5375.55	−5375.55	−5375.56
5	−5292.34	−5292.40	−5292.39	−5292.42	−5292.43	−5292.43

Table 4 Hamiltonian model parameters E_o and Js for each sample (in eV, *values in brackets* represent the standard error in the last figure, distances are in Å)

Parameter	Distance	1	2	3	4	5
E_o		−5300.45 (66)	−5299.42 (61)	−5222.25 (71)	−5376.14 (8)	−5292.83(15)
J_1	< 3.3	0.656 (16)	0.652 (14)	0.620 (18)	0.025 (2)	0.015 (3)
J_2	5.1–5.3	0.168 (10)	0.162 (10)	0.151 (11)	0.007 (1)	0.005 (2)
J_3	5.8–6.2	0.089 (11)	0.088 (10)	0.066 (12)	0.003 (1)	0.008 (3)
J_4	7.7–8.2	0.025 (8)	0.015 (9)	0.030 (9)	0.003 (1)	0.001 (2)

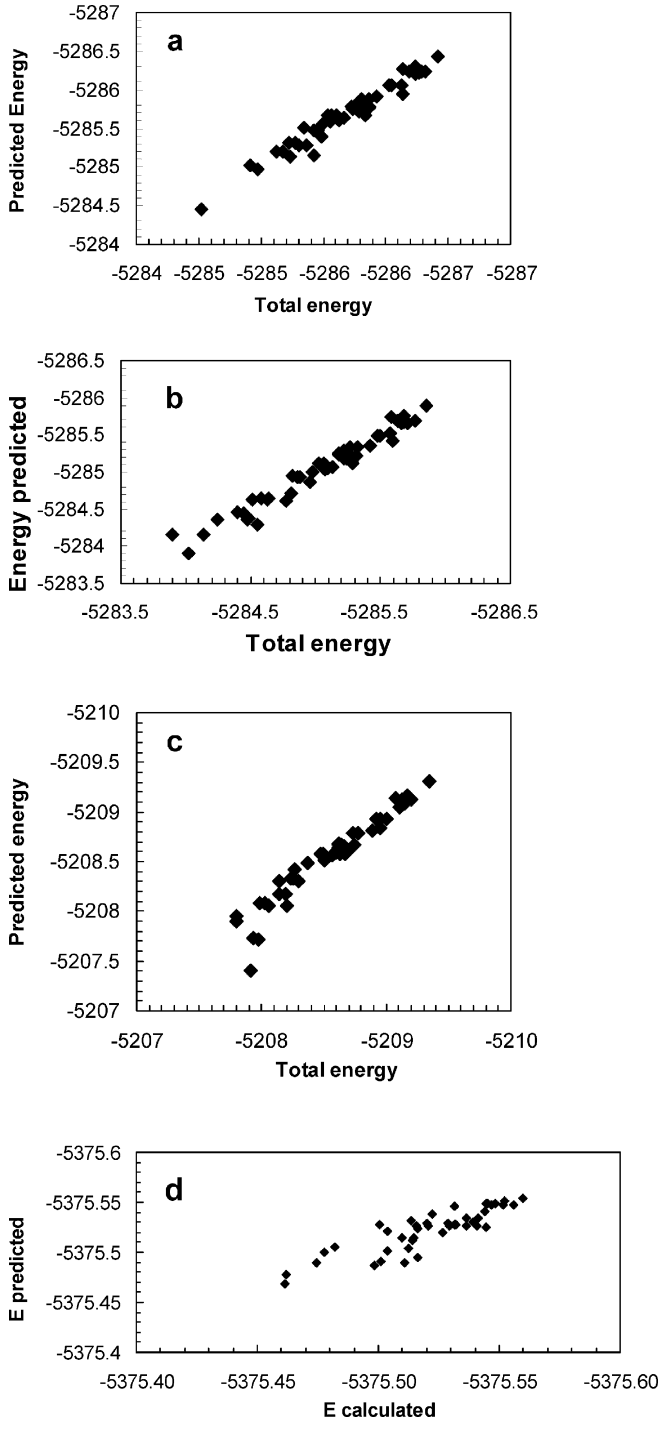

Fig. 3a–d Relationship between lattice energy of configurations with different octahedral cation arrangement and the predicted values with the Hamiltonian model. Samples *1* (**a**), *2* (**b**), *3* (**c**) and *4* (**d**)

and the tetrahedral charge variation did not produce significant changes in the exchange interaction values (J_i). The high and positive values of J_1 indicate that the AlAl and MgMg are likely to be dispersed. In the Al/Fe system (samples 4 and 5), the J_i values are significantly lower than in the Al/Mg system, showing no significant ordering preference. The substitution of Mg^{2+} creates a local negative charge and the relative position of these cations is important, hence the J values in the Al/Mg system are significantly higher than in the Al/Fe samples, where the substitution of Fe^{3+} does not create this negative charge.

MC simulations

Mg/Al system

With these Js in our Hamiltonian model, we performed MC simulations for a proportion Al/Mg = 1/1. One order–disorder phase transition was detected, observing a change in the heat capacity during the cooling process in the MC simulation (Fig 4a). This change comes with a drastic variation in the proportion of the number of J, interactions, indicating that a phase transition is produced. (Fig. 4b). Different sampling configurations of the octahedral Mg/Al distribution were taken, observing the transition from a disordered structure, through a partially ordered state containing domain walls, to a completely ordered configuration, where no AlAl or MgMg pairs as first neighbours were found (Fig. 5a–c). All Al/Mg samples (1–3) produce the same order–disorder phase transition, the same ordered structure and at similar temperature.

We extended the simulations for a proportion Al/Mg = 3/1 for sample 1. An order–disorder transition was also detected (Fig. 6). In Fig. 7, different configurations sampled during the MC simulations are represented. Again, the system evolves from disordered (Fig. 7a) through partially ordered state with domain walls (Fig. 7b) to a fully ordered state (Fig. 7c and d). In the ordered state, atoms are arranged in chains via J_3 interactions, and adjacent chains are linked by J_4 interactions, forming a zig-zag pattern, which is marked for clarity in Fig. 7c. These simulations were extended for samples 2 and 3. Similar order–disorder phase transitions were detected at the same temperature. The ordered structures are also similar to those found for sample 1, although some domain walls with superhexagon structures of Mg have been detected for sample 3.

Al/Fe system

We performed simulations for composition Al/Fe = 3/1 in sample 4, in which a phase transition was once again detected, observing a peak in the heat capacity (Fig. 8). The system shows an ordering scheme similar to that for the analogous Al/Mg system, except that the J_3 chains are now linked by J_3 interactions. Figure 9a, and b shows configurations which are disordered and fully ordered, respectively. The ordering temperature T_c for this system is 1 order of magnitude lower than that in the Al/Mg systems; this is due to the fact that the Al/Fe Js are much smaller than those for Al/Mg. Nevertheless, an

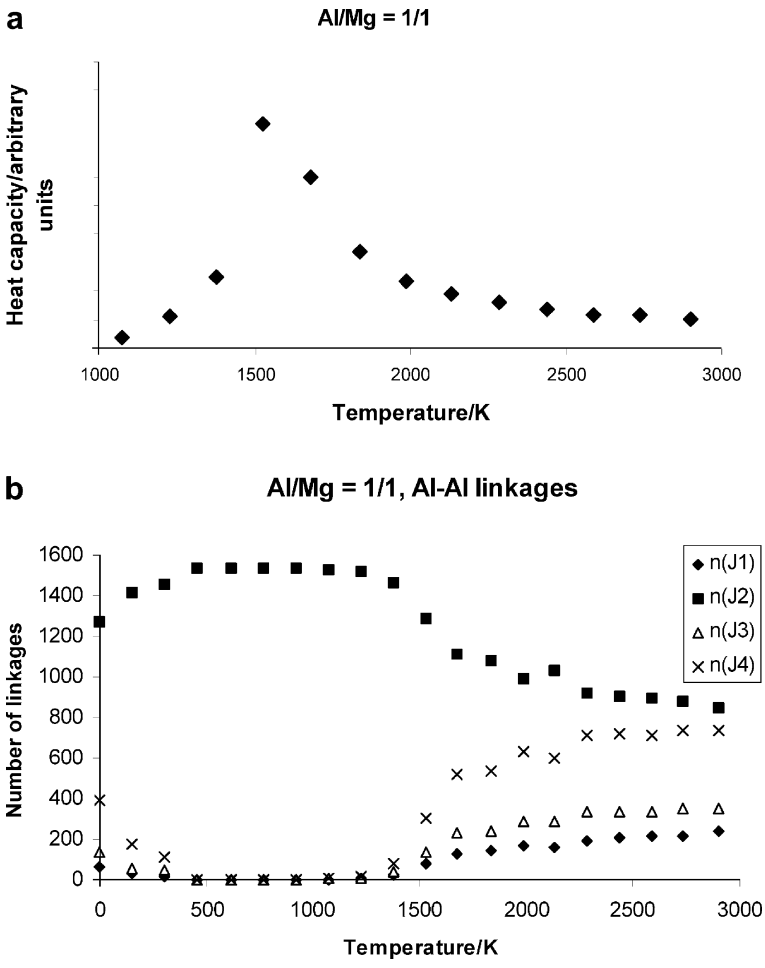

Fig. 4a, b MC results for simulations of the octahedral Al/Mg distribution for Al/Mg = 1/1, heat capacity variation with temperature (**a**), evolution of the numbers of each type of J linkage for each type of atom, $n(J_{n,i-i})$, as a function of temperature (**b**)

ordered configuration like that described in Fig. 7c will be likely to be among the ordered structures, although it was not found. This configuration is controlled by J_3 and J_4 interactions and $J_3 = J_4$ in this sample. Hence, this configuration will have energy similar to that found in the MC simulations (Fig. 9b). This simulation was also performed for sample 5, detecting also an order–disorder phase transition at low temperature. However, this sample 5 does not show long-range order. Nevertheless, short-range order is detected with Fe–Fe interactions across J_2 distances (Fig. 9c).

Discussion

In the Mg/Al system with an octahedral cation proportion Al/Mg = 3/1, the minimum energy structure corresponds to a completely ordered configuration. This structure was not included in the initial configuration set used for calculating the exchange interaction values. This ordered configuration presents Mg chains with a zig-zag pattern slightly dephased with respect to each other, that is controlled by J_3 and J_4 interactions (Fig. 7c). In addition, another similarly ordered configuration, also with zig-zag Mg chains but in phase pattern, was found in sample 3 (Fig. 7d). In this ordered distribution the Mg cations form hexagons or superstructures with an additional order degree at long range. This distribution is only controlled by the J_3 interactions. However, the total energy of an optimized $2 \times 2 \times 1$ supercell of this last configuration was calculated showing it to have the lowest energy of the initial ordered distributions included in the exchange interaction calculation set (Table 3), for different compositions (−5286.47 eV and −5209.39 eV for 1 and 3, respectively). To validate this MC simulation, a total energy calculation and optimization of the most stable ordered configuration obtained in this simulation (Fig. 7c) was performed, although this configuration is difficult to represent in a $2 \times 2 \times 1$ supercell due to the dephased zig-zag pattern of the Mg chains. Nevertheless, it can be represented by a $4 \times 4 \times 1$ supercell. Therefore, $4 \times 4 \times 1$ supercells (660 atoms) of these both ordered configurations (Fig. 7c,d) were calculated, obtaining a similar energy for both configurations. The distribution of Fig. 7c is only 0.05 eV/unit cell^{-1} more stable than that of Fig. 7d. This fact can be explained from the J values. The configuration of Fig. 7d is controlled only by J_3 interactions, whereas that of Fig 7c is controlled by J_3 and J_4 interactions, being $J_3 > J_4$ in all Al/Mg samples. Therefore, the configuration of Fig. 7c will have lower energy than that of figure 7d, and this last

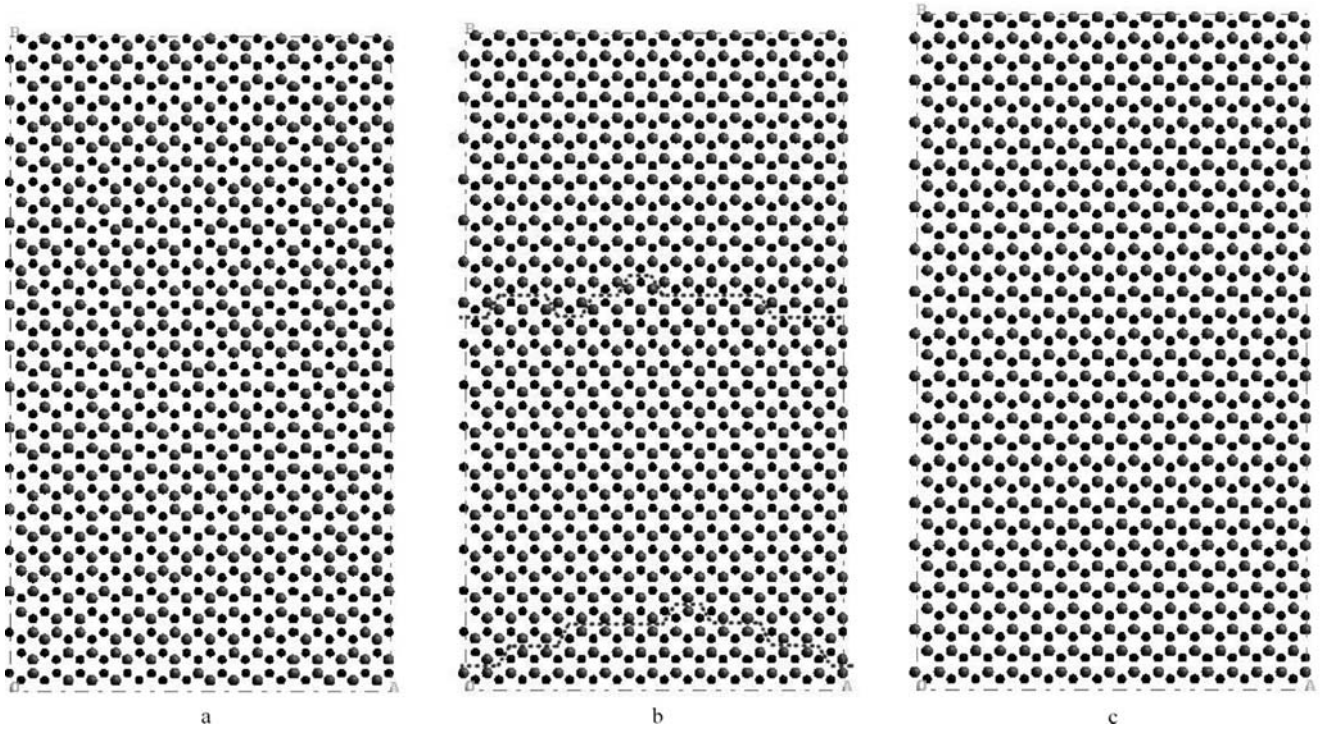

Fig. 5a–c Snapshots during the MC simulation of the Al/Mg distribution in the octahedral sheet (Al/Mg = 1/1). A disordered distribution (**a**), through an intermediate distribution (**b**) containing domain walls (marked with *dotted lines*) and an ordered configuration (**c**). *Black* and *dark grey spheres* represent Al and Mg cations, respectively

configuration was detected only in sample 3 where J_3 has the lowest value and the J_4 has the highest value of the Al/Mg samples (Table 4).

This fact validates the procedure used for calculating the exchange interaction parameters. In this minimum energy structure (Fig. 7c), the Mg are maximally dispersed. In samples with 50% Mg in the octahedral sheet (octahedral composition, Al/Mg 1/1), the minimum energy structure corresponds also to an ordered distribution where the Mg are also maximally dispersed. The presence of MgMg pairs as first or second neighbours produces geometrical distortions in the octahedral sheet due to the higher radius of Mg^{2+} (0.65 Å) with respect to Al^{3+} (0.5 Å). Moreover, the octahedral charge is produced by the Mg^{2+} substitution in our system. A localized concentration of negative charge in the octahedral sheet would locally destabilize the structure. In our minimum energy configuration, the octahedral charge is homogeneously dispersed. The Al/Mg exchange interaction values do not change significantly with the variation of tetrahedral charge or interlayer cation (Na^+ or K^+). Therefore, the ordering of Al/Mg cations in the octahedral sheet will be similar for smectites and illites. This result agrees with the experimental fact found in illite/smectite samples that no MgMg cation pair was detected (Cuadros and Altaner 1998; Cuadros et al. 1999). Previous reverse MC simulations based on FT–IR and ^{27}Al–NMR experimental data presented that the Mg^{2+} cations are highly dispersed along the octahedral sheet of illites and smectites, finding some domains with distributions of Mg ordered similarly to those shown in Fig. 7c and d (Sainz-Díaz et al. 2001b). We can consider that these natural samples have not yet reached the equilibrium state, presumably because of kinetic constraints, and only intermediate distributions are detected. On the other hand, these experimental data are based on mean values of configurations from different layers that are not perfectly ordered in the stacking process. Hence, it will be difficult to find experimentally the low-energy ordered configurations in these natural minerals.

In the Al/Fe system with an octahedral cation composition Al/Fe 3/1, the most stable distribution is also an

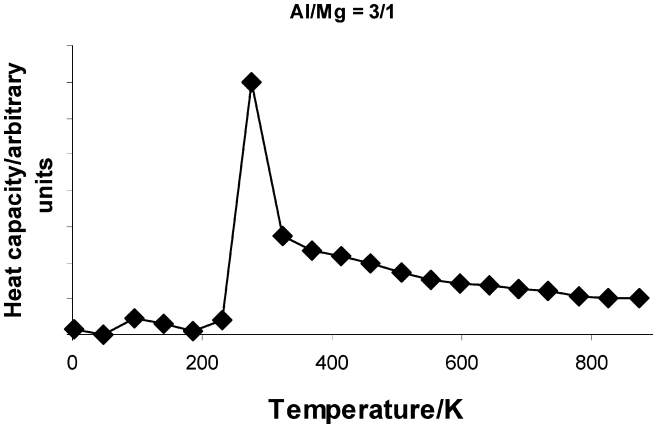

Fig. 6 Variation of the heat capacity with temperature during the MC simulations of the Al/Mg octahedral cation distribution (Al/Mg = 3/1)

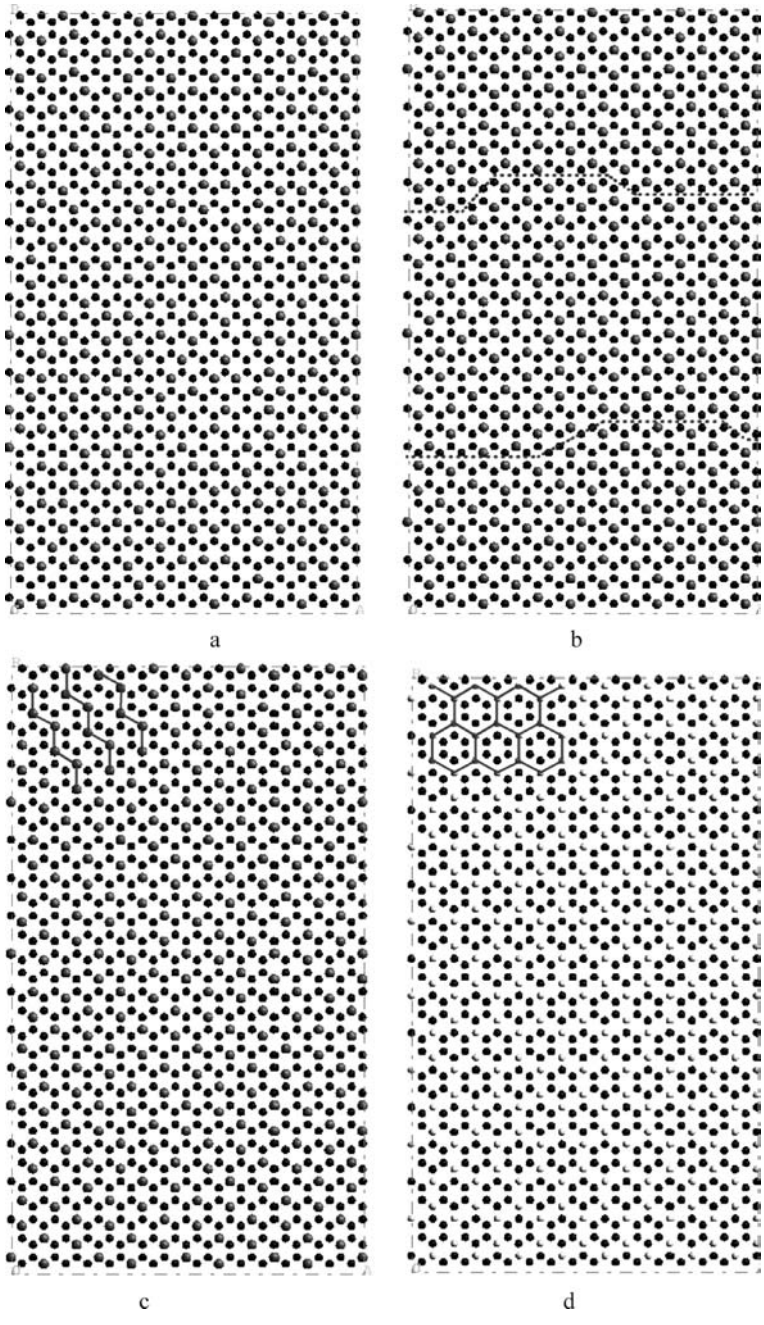

Fig. 7a–d Configurations of the octahedral sheet during the MC simulation of the Al/Mg cation distribution (Al/Mg = 3/1). A disordered distribution (**a**), an intermediate distribution containing domain walls (marked with *dotted lines*) (**b**), and completely ordered configurations (**c** and **d**). *Black and grey spheres* represent Al and Mg cations, respectively

ordered one. This structure was optimized and the total energy calculations confirmed that it is one of the most stable configurations. However, the exchange interaction parameters J are too small and the phase transition temperature is low. This means that the energy passing from an ordered to a disordered distribution is low. Hence, this disperse ordered distribution for Fe in the octahedral sheet will rarely be observed in natural samples of dioctahedral clays. This is consistent with experimental studies on synthetic smectites, where Al ▶

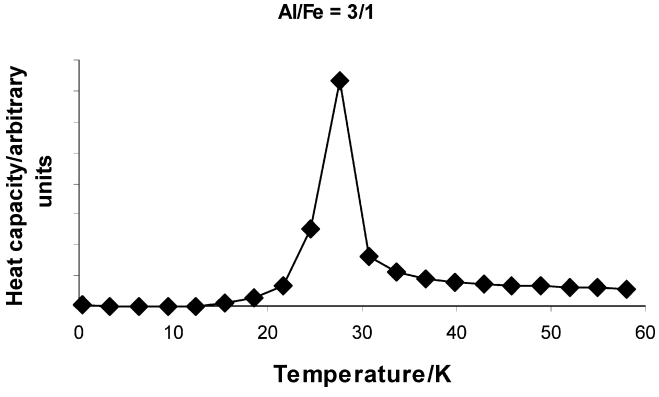

Fig. 8 Variation of the heat capacity with temperature during the MC simulations of the Al/Fe octahedral cation distribution (Al/Fe = 3/1)

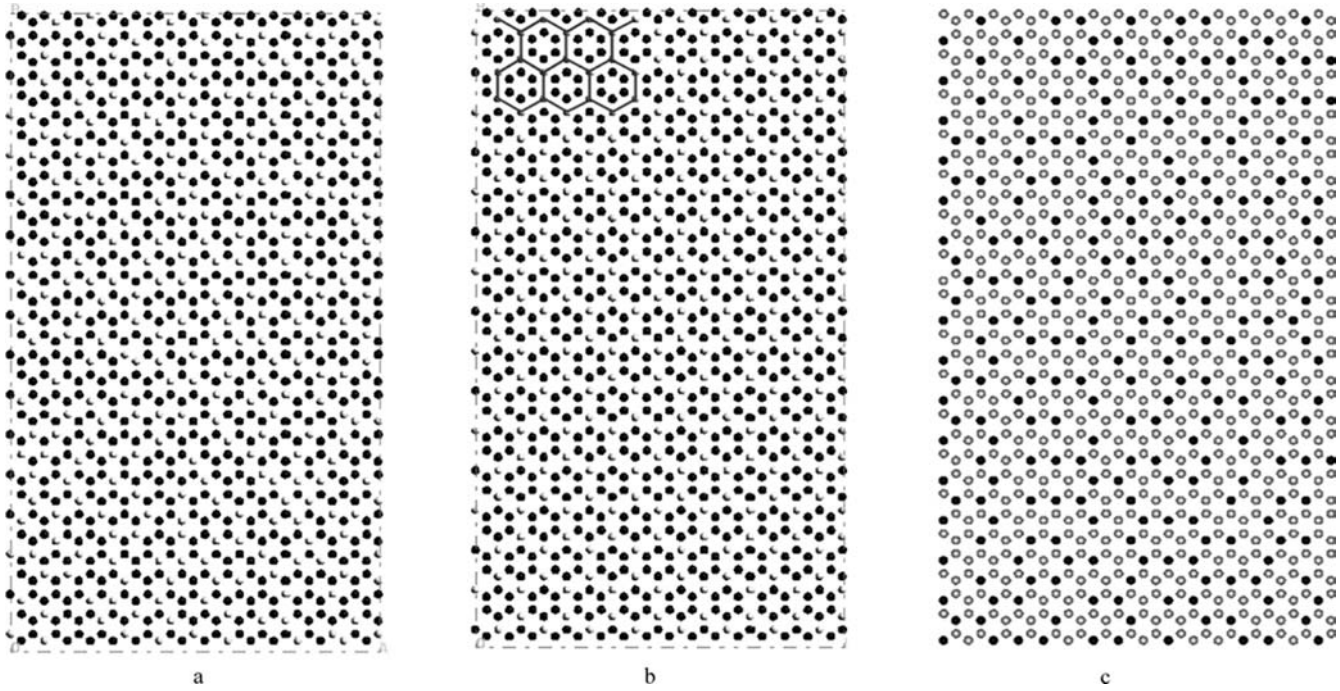

Fig. 9a–c Configurations of the octahedral sheet during the MC simulation of the Al/Fe cation distribution (Al/Fe = 3/1). A disordered distribution (**a**), and completely ordered configurations of samples *4* (**b**) and *5* (**c**). In graphs **a** and **b**, *black* and *grey spheres* represent Al and Fe cations, respectively. In graph **c**, *grey and black spheres* represent Al and Fe cations, respectively

and Fe tend to mix rather than to segregate (Grauby et al. 1991; Decarreau et al. 1992). The increase in interlayer charge produces a different J set except J_3 that is slightly higher. Hence, the tendency to a dispersely ordered distribution will be slightly lower in samples with higher interlayer charge. In similar systems, shale illite–smectite samples, Schroeder (1993) found that Fe also mixes with Al in samples with low Fe content.

On the contrary, in dioctahedral clays with a higher Fe content and in presence of Mg, a tendency of Fe to segregate is observed experimentally in the octahedral sheet (Sainz-Díaz et al. 2001b). Hence, the models studied in this work cannot describe these natural minerals. Probably the presence of Mg helps the Fe cations to be segregated. Moreover, the peculiar electronic structure of Fe should play some role in the distribution tendency of these cations. Obviously, this electronic structure is not included in the methodology used in this work, and quantum-mechanical calculations would be useful to clarify this point. Further investigations on the effect of Mg presence in the Al/Fe system and more complex systems including the quantum-mechanical approach will be performed.

Acknowledgements The authors are grateful to J. Gale for permitting us to use the GULP program, V. Botella for fruitful discussions, J. Ruiz-García for his help and for the financial support of NERC (M.T. Dove), EPSRC (E. Palin), the Royal Society, UK and the MEC, Spain (C.I. Sainz-Díaz), and the PB97-1205 and BTE2000-1146-CO2-01 MCYT projects and Acciones Integradas UK/Spain joint research programme.

References

Abbot RN Jr, Post JE, Burnham CW (1989a) Treatment of the hydroxyl in structure–energy calculations. Am Mineral 74: 141–150

Abbot RN Jr, Burnham CW, Post JE (1989b) Hydrogen in humite-group minerals: structure–energy calculations. Am Mineral 74: 1300–1306

Besson G, Drits VA, Daynyak LG, Smoliar BB (1987) Analysis of cation distribution in dioctahedral micaceous minerals on the basis of IR spectroscopy data. Clay Miner 22: 465–478

Bosenick A, Dove MT, Geiger CA (2000) Simulation studies of pyrope–grossular solid solutions. Phys Chem Miner 27: 398–418

Bosenick A, Dove MT, Myers ER, Palin E, Sainz-Díaz CI, Guiton B, Warren MC, Craig MS, Redfern SAT (2001) Computational methods for the study of energies of cation distributions: applications to cation-ordering phase transitions and solid solutions. Mineral Mag 65: 197–223

Bush TS, Gale JD, Catlow CRA, Battle PD (1994) Self-consistent interatomic potentials for the simulation of binary and ternary oxides. J Mater Chem 4: 831–837

Collins DR, Catlow CRA (1992) Computer simulations of structures and cohesive properties of micas. Am Mineral 77: 1172–1181

Cuadros J, Altaner SP (1998) Compositional and structural features of the octahedral sheet in mixed-layer illite/smectite from bentonites. Eur J Mineral 10: 111–124

Cuadros J, Sainz-Díaz C, Ramírez R, Hernández-Laguna A (1999) Analysis of Fe segregation in the octahedral sheet of bentonitic illite–smectite by means of FT–IR, ^{27}Al MAS NMR and reverse Monte Carlo simulations. Am J Sci 299: 289–308

Decarreau A, Grauby O, Petit S (1992) The actual distribution of octahedral cations in 2:1 clay minerals: results from clay synthesis. Appl Clay Sci 7: 147–167

Dove MT, Heine V (1996) The use of Monte Carlo methods to determine the distribution of Al and Si cations in framework aluminosilicates from ^{29}Si MAS NMR data. Am Mineral 81: 349–362

Dove MT, Cool T, Palmer DC, Putnis A, Salje EKH, Winkler B (1993) On the role of Al/Si ordering in the cubic-tetragonal phase transition in leucite. Am Mineral 78: 486–492

Dove MT, Thayaparam S, Heine V, Hammonds KD (1996) The phenomenon of low Al–Si ordering temperatures in aluminosilicates framework structures. Am Mineral 81: 349–362

Drits VA, Dianyak LG, Muller F, Besson G, Manceau A (1997) Isomorphous cation distribution in celadonites, glauconites and Fe-illites determined by infrared, Mössbauer and EXAFS spectroscopies. Clay Miner 32: 153–179

Gale JD (1997) GULP – a computer program for the symmetry-adapted simulation of solids. J Chem Soc Faraday Trans 93: 629–639

Grauby O, Petit S, Decarreau A (1991) Distribution of Al–Fe–Mg in octahedral sheets of synthetic smectites: study of three binary solid-solutions. Proceedings 7th EUROCLAY Conference Dresden 441–446

Grauby O, Petit S, Decarreau A, Baronnet A (1993) The beidellite-saponite series: an experimental approach. Euro J Mineral 5: 623–635

Herrero CP (1993) Monte Carlo simulation of the Al, Si distribution in A-type zeolites. J Phys Chem 97: 3338–3343

Herrero CP, Sanz J (1991) Short-range order of the Si, Al distribution in layer silicates. J Phys Chem Solids 52: 1129–1135

Herrero CP, Ramírez R (1992) Energetics of cation ordering in the Faujasite framework: Monte Carlo simulations. J Phys Chem 96: 2246

Jackson RA, Catlow CRA (1988) Computer simulation studies on zeolite structures. Mol Simul 1: 207–224

Morris HD, Bank S, Ellis PD (1990) ^{27}Al NMR spectroscopy of iron-bearing montmorillonite clays. J Phys Chem 94: 3121–3129

Muller F, Besson G, Manceau A, Drits VA (1997) Distribution of isomorphous cations within octahedral sheets in montmorillonite from Camp-Bertaux. Phys Chem Miner 24: 159–166

Palin EJ, Dove MT, Redfern SAT, Bosenick A, Sainz-Díaz CI, Warren MC (2001) Computational study of tetrahedral Al-Si ordering in muscovite. Phys Chem Miner 28: 534–544

Post JE, Burnham CW (1986) Ionic modeling of mineral structures and energies in the electron gas approximation: TiO_2 polymorphs, quartz, forsterite, diopside. Am Mineral 71: 142–150

Sainz-Díaz CI, Hernández-Laguna A, Dove MT (2001a) Modelling of dioctahedral 2:1 phyllosilicates by means of transferable empirical potentials. Phys Chem Miner 28: 130–141

Sainz-Díaz CI, Cuadros J, Hernández-Laguna A (2001b) Analysis of cation distribution in the octahedral sheet of dioctahedral 2:1 phyllosilicates by using inverse Monte Carlo methods. Phys Chem Miner 28: 445–454

Schröder K-P, Sauer J, Leslie M, Catlow CRA, Thomas JM (1992) Bridging hydroxyl groups in zeolitic catalysts: a computer simulation of their structure, vibrational properties and acidity in protonated faujasites (H-Y zeolites). Chem Phys Lett 188: 320–325

Schroeder PA (1993) A chemical, XRD, and ^{27}Al MAS NMR investigation of Miocene Gulf Coast shales with application to understanding illite-smectite crystal chemistry. Clays Clay Miner 41: 668–679

Thayaparam S, Heine V, Dove MT, Hammonds KD (1996) A computational study of Al/Si ordering in cordierite. Phys Chem Miner 23: 127–139

Tsipursky SI, Drits VA (1984) The distribution of octahedral cations in the 2:1 layers of dioctahedral smectites studied by oblique-texture electron diffraction. Clay Miner 19: 177–193

Warren MC, Dove MT, Myers ER, Bosenick A, Palin EJ, Sainz-Diaz CI, Guiton B, Redfern SAT (2001) Monte Carlo methods for the study of cation ordering in minerals. Mineral Mag 65: 225–252

Winkler B, Dove MT, Leslie M (1991) Static lattice energy minimization and lattice dynamics calculations on aluminosilicate minerals. Am Mineral 76: 313–331